Characteristics of the rotor R4-01 for the O4 NCal system VIR-0591C-22

Eddy Dangelser, Dimitri Estevez, Hubert Kocher, Benoit Mours,
Mehmet Ozturk, Antoine Syx

IPHC-Strasbourg

September 8, 2022

Contents

This note is a revised version of the previous release, we investigated the remaining 1f signal induced by the counterweight and explained where this signal comes from by adjusting the geometry of the rotor using additionnal measurements. The new predicted signal at twice the rotor frequency remains within the uncertainties of the previous version of the note with now reduced uncertainties.

1 Introduction

The challenge of the NCal system for O4 is to improve the NCal signal uncertainty. This can be achieved by reducing uncertainties on the rotor parameters such as the density of the material discussed in VIR-0160A-22, the thickness or the radius of the sectors.

Figure 1 shows an isometric view and pictures of both faces of the O4 rotor design. The drawings are attached at the end of this note.

The rotor has been engraved IPHC-R4-01 on a side and sandblasted on the other side as shown in figure 2.

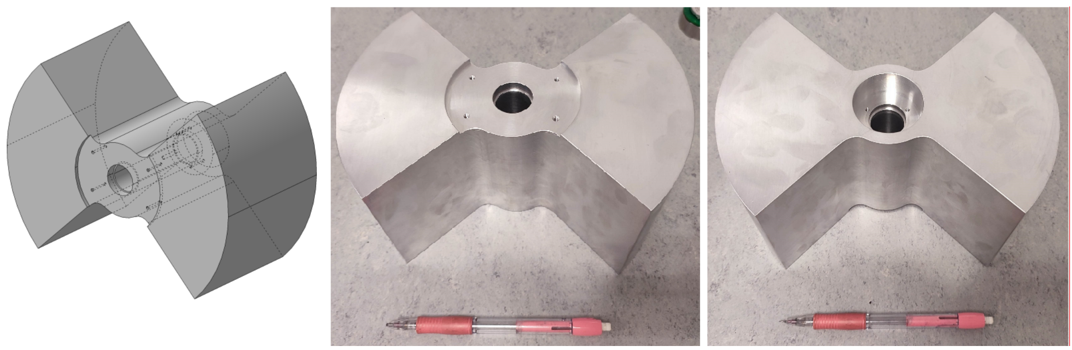

Figure 1: From left to right, isometric view of the rotor, picture of the up face, picture of the down face.

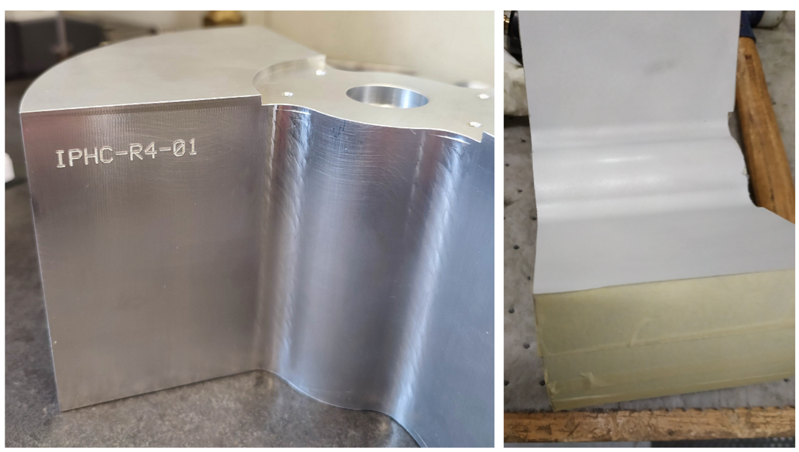

Figure 2: Left shows the engraving made on a side of the rotor, right shows the sandblasting made on the other side.

2 Measurement method

To determine the geometry of the rotor, several measurement points were used to compute the thickness of the sectors as shown in figure 3. Since the strain on the mirror induced by the rotor will come from the sectors, we need to measure the thickness of both sectors as well as the outer and inner diameters. The central part is not affecting the signal since it is a full cylinder. The outer diameter was measured in 4*2 = 8 points and the inner diameter using 4 points.

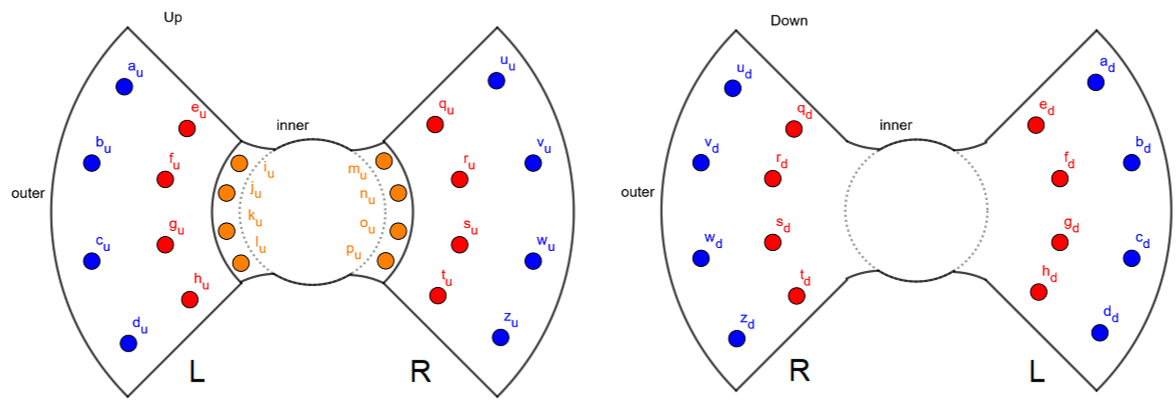

Figure 3: Outline of the faces of the rotor with the measurement points. Left figure is face up, right figure is face down. Sectors have been labelled L for left sector and R for right sector.

The tool used to measure the thickness and the outer diameter is a measuring column "DIGIMAR CX1" (see VIR-0160A-22) with a given precision of 2+L/600 μm (L the measured length in mm). A vernier caliper "TESA-CAL IP67" with a precision of 20 μm was used to measure the inner diameter.

The measuring column is operated on a metrology table, different measurements were made to check the flatness on a surface roughly equivalent to the rotor layout. The value range from 0 to 7 μm. The rms of the 11 values is 2.0 μm.

We measured the opening angles of the sectors using a video measuring microscope "Garant MM2" (see fig. 20) with a given precision of 2.9+L/100 μm at 95% CL (L the measured length in mm).

2.1 Thermal effects and density

As discussed in VIR-0160A-22, the thermal effects on the aluminum 7075 must be taken into account (23.6 μm/m/°C).

A reference temperature of 21.5°C was chosen to express the density of the material. The temperature inside the NE building might fluctuate around 21.5°C. The temperature of the motor can increase by up to several tens of degrees depending on the rotation speed. This will increase the rotor temperature. The strains computation has been made assuming a reference temperature of 23°C. They will have to be corrected using eq. (2) for the true operating temperature. We expect to know this temperature with an uncertainty of ± 3°C.

The uncertainty on the strain h is the following:

$$\begin{aligned} h &\propto \rho_{rot}\, b\, r_{max}^4 \\ &\propto \frac{m\, r_{max}^2}{\pi} \end{aligned} \tag{1}$$

Using $r(T) = r(1 + \alpha_T)$ (with the temperature factor $\alpha_T = C_T(T - T_{ref})$) we have:

$$\begin{aligned} h(T) &\propto r^2_{max}(T) \\ &\propto r^2_{max}(1 + \alpha_T)^2 \end{aligned} \tag{2}$$

We compute the relative uncertainty of h on the temperature T:

$$\left|\frac{\partial h}{\partial T}\right| \frac{\Delta T}{h} = \frac{2C_T}{1 + C_T(T - T_{ref})}\Delta T \tag{3}$$

The density of the rotor R4-01 is then 2808.1 $\pm$ 0.2 kg.m^{-3}. This density is measured in air, if the rotor is used under vacuum, the density should be increased by the air density (ρ_{air}=1.3 kg.m^{-3}).

3 Raw measurements of the rotor

This section presents the raw measurements made on the rotor at the ambient temperature of 20.1°C. Table 1 shows the thickness measurements according to the measurement points defined in figure 3. The rotor is laying on the table. The rotor surface as well as the table are not perfectly flat. Some space could be present in between that should be substracted when computing the rotor thickness as discussed later.

Measurement point	L sector		Measurement point	R sector	
	Up	Down		Up	Down
a	104.353	104.339	q	104.319	104.314
b	104.338	104.330	r	104.309	104.308
c	104.325	104.316	s	104.303	104.302
d	104.312	104.302	t	104.299	104.300
e	104.325	104.325	u	104.326	104.326
f	104.314	104.314	v	104.316	104.315
g	104.308	104.308	w	104.303	104.303
h	104.304	104.306	z	104.292	104.294
i	101.269		m	101.262	
j	101.262		n	101.256	
k	101.257		o	101.251	
l	101.252		p	101.248	

Table 1: Raw measurements of the height in mm for each point at 20.1°C on L and R sectors of R4-01.

Table 2 displays the diameter measurements. The measurements were made on 4*2 diameters (two parts of each diameter, the up and down sides of the rotor).

Measurement point	Up	Down
1	208.046	208.055
2	208.047	208.060
3	208.054	208.053
4	208.044	208.057

Table 2: Raw measurements of the diameter in mm for each point at 20.1°C on R4-01.

Measurements were made on the inner radius r_{min} = 28.93 mm and the up face radius for the counterweight $r_{\text{counterweight}}$ = 39.99 mm. These values were measured using the vernier caliper and are the same for a temperature of 23°C.

4 Extracting the geometrical parameters

4.1 Thickness

We need to correct the possible gap between the rotor and the measuring table. Assuming that the table is flatter than the rotor surface we can extract the gap from the measurement of the top surface considering the plane tangents to the highest points (asking them to be on both sectors). For this rotor these points are a, b and u from figure 3. Using the measurements in table 1 we can compute a plane equation for each side of the rotor in cartesian coordinates:

$$\text{Up plane equation} : z = -1.85 \times 10^{-4}x + 5.49 \times 10^{-4}y + 104.32 \quad (4)$$

$$\text{Down plane equation} : z = -8.83 \times 10^{-5}x + 3.21 \times 10^{-4}y + 104.33 \quad (5)$$

Using eqs. (4) and (5) the gap can be determined, see table 3. The maximum rms of the gap for each sector is 8.3 μm.

Measurement point	L sector		Measurement point	R sector	
	Up	Down		Up	Down
a	0	0	q	9	2
b	0	0	r	7	-1
c	3	-6	s	6	-7
d	6	-13	t	3	-12
e	6	13	u	0	0
f	11	15	v	0	-10
g	10	9	w	1	-16
h	5	0	z	1	-20

Table 3: Gap computed in μm on up and down sides of both sectors of R4-01.

We can then compute the rotor thickness for each point by removing these gaps. If one of the raw values is lower than the corrected thickness we take this lowest value. The value of each point is shown in table 4 at 21.5°C.

Measurement point	L sector	Measurement point	R sector
a	104.346	q	104.321
b	104.337	r	104.315
c	104.317	s	104.303
d	104.296	t	104.295
e	104.332	u	104.333
f	104.321	v	104.312
g	104.315	w	104.294
h	104.311	z	104.281
i	101.276	m	101.269
j	101.269	n	101.263
k	101.264	o	101.258
l	101.259	p	101.255

Table 4: Measurements of the thickness in mm for each point at 23°C on L and R sectors of R4-01.

4.2 Radius

Using comparators while the rotor is rotating on its axis we can determine the deformation on both sectors and compute different radii values. Table 5 shows the raw measurements using comparators on L and R sectors. The measurements were made on the up and down sides of L and R sectors using two comparators for a total of 5*2*2=20 points (the first and last points are near the edge of the sectors).

Measurement point	L sector		R sector	
	Up	Down	Up	Down
A	0	-5	20	0
B	20	10	25	0
C	30	20	35	0
D	20	10	0	0
E	0	-5	0	0

Table 5: Raw measurements in μm of the comparators for the L and R sectors of R4-01.

The zeroing of the comparators was made arbitrarily close to the edge of the sector. The offsets shown in table 5 are measured relative to this reference.

To compute the radius per measurement point we use the following process: First we compute the mean deformation for one comparator. Then we remove this mean deformation to each measurement of this comparator. The corrected shift value is added to the mean radius of 104.029 mm computed using table 2 at 21.5°C. This process is repeated for each comparator. The final radius for each point are shown in table 6.

Measurement point	L sector		R sector	
	Up	Down	Up	Down
A	104.007	104.006	104.027	104.021
B	104.027	104.021	104.032	104.031
C	104.037	104.031	104.042	104.036
D	104.027	104.021	104.032	104.031
E	104.007	104.006	104.027	104.021

Table 6: Radius measurements in mm at 20.1°C for the L and R sectors of R4-01.

We found the sectors to be in an elliptical shape as shown in an amplified representation in figure 4. The general shape of up and down sectors is represented as one unique radius for this representation.

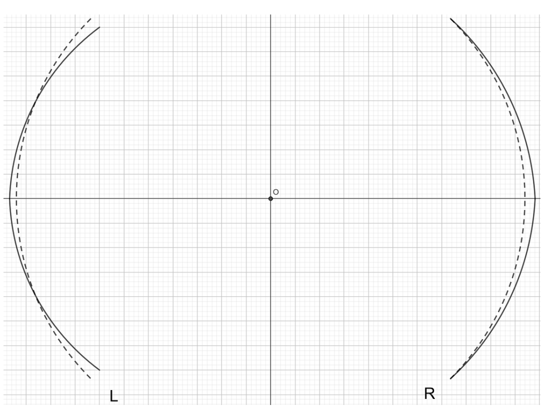

Figure 4: Outline of the shape of the L and R sectors radii. The dashed lines represent the mean diameter of the rotor, the plain lines represent the amplified deformation determined using comparators.

5 Characterization of the rotor using a simple model

5.1 Theoretical model of the rotor

Using the drawing values of the rotor we have a thickness of 104.4 mm and a radius of 104 mm for both sectors.

Using FROMAGE v1r2 (see VIR-0759B-20) we compute a theoretical value for the rotor with these values. A config file used to compute an advanced rotor model is shown at the end of this note. We obtain the following 2f strain signal:

$$\text{strain}(2\text{f}) = \frac{2.1198 \times 10^{-18}}{(2f_{rot})^2}$$

This strain value will be compared to models based on the measurements of the rotor.

5.2 Thickness

A simple model can be used to determine a mean value for the thickness and its uncertainty.

As shown on figure 3, a total of 16 points were used to compute the thickness of each sector. In this case we will not consider the inner points so that we obtain uniform sectors.

For the simple model we take the thickness as the mean value of table 4: 104.314 mm at 23°C. Since we have a limited number of measurement points, to be conservative we take the thickness uncertainty as the rms of table 4 (17.6 μm) to which we add linearly the metrology table uncertainty (2 μm) and the tool uncertainty (2.2 μm). Therefore, for this simple model, the thickness is 104.314 $\pm$ 0.022 mm.

5.3 Radius

For the simple model we take the radius as the mean value of table 6: 104.033 mm at 23°C. Using a linear sum of the rms of table 6 (10.6 μm) and the tool uncertainty (2.4 μm) we take an uncertainty of 12.9 μm on the mean radius.

We have to point out that we do not take into account the fact that the sectors might not be centered on the same axis. Therefore the uncertainty might be underestimated. We will then consider each sector individually later.

5.4 Expected NCal signal and uncertainties

The geometry used to describe the rotor as a simple model is represented in figure 5.

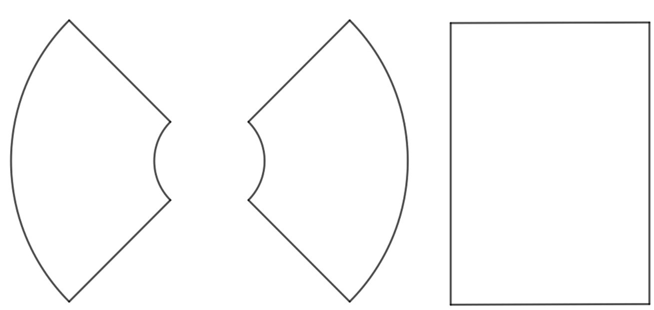

Figure 5: Simple model geometry used to describe the rotor. Left is a front view, right is a side view.

Using the analytical equation of the strain at 2f (see eq.8 in Newtonian calibrator tests during the Virgo O3 data taking):

$$\text{strain(2f)} = \frac{9G\rho_{rot}\ b\ \sin(\alpha)(r_{max}^4 - r_{min}^4)}{32\pi^2(2f)^2 d^4 L}\cos(\phi)\Bigg[1 + \frac{25}{54d^2}\frac{(r_{max}^6 - r_{min}^6)}{(r_{max}^4 - r_{min}^4)} + \left(\frac{45}{8}\sin(\phi)^2 - \frac{5}{2}\right)\left(\frac{r_{mir}}{d}\right)^2 + \left(\frac{15}{8}\cos(\phi)^2 - \frac{25}{24}\right)\left(\frac{x_{mir}}{d}\right)^2 - \frac{25}{72}\left(\frac{b}{d}\right)^2\Bigg] \quad (6)$$

with:

- G the gravitationnal constant
- ρ_{rot} the density of the rotor
- b the thickness of the rotor
- α the opening angle of the rotor
- r_{max} and r_{min} the outer and inner radius of the rotor
- f the rotor frequency
- ϕ the rotor angle from the beam axis
- L the interferometer arm length
- r_{mir} the radius of the mirror
- x_{mir} the thickness of the mirror

We compute with our parameters (d = 1.7 m and an angle ϕ = 34.7°): strain(2f) $= \dfrac{2.1208 \times 10^{-18}}{(2f_{rot})^2}$.

Using FROMAGE on this geometry we compute the following strains on the mirror at a distance of 1.7m and an angle of 34.7°:

- strain(1f) $= \dfrac{1.28 \times 10^{-30}}{(1f_{rot})^2}$
- strain(2f) $= \dfrac{2.1210 \times 10^{-18}}{(2f_{rot})^2}$
- strain(3f) $= \dfrac{1.76 \times 10^{-30}}{(3f_{rot})^2}$

We notice that the 2f strain signal has the largest amplitude at 10^{-18}. Both sectors being the same height and radius the only expected siginificant signal is the 2f. The 1f and 3f strain signals are at the level of the numerical noise of the simulation. This result is in agreement with a simple rotor model.

Comparing the theoretical model strain with the simple model at 2f using FROMAGE we obtain a relative deviation of 0.057%.

Comparing the analytical strain (eq. (6)) at 2f with FROMAGE we obtain a relative deviation of 0.009%.

The uncertainties considered on the 2f signal for this model are displayed in table 7.

R4-01 rotor parameter simple model (23°C)			NCal 2f signal uncertainty	
name	value	uncertainty	formula	value (%)
Density ρ (kg.m^{-3})	2808.1	0.2	$\delta\rho/\rho$	0.007
Thickness b (mm)	104.311	2.2×10^{-2}	$\delta b/b$	0.021
r_{max} (mm)	104.029	1.3×10^{-2}	$4\delta r_{max}/r_{max}$	0.050
G (m^3.kg^{-1}.s^{-2})	$6.674\,30 \times 10^{-11}$	1.5×10^{-15}	$\delta G/G$	0.002
Temperature T (°C)	23	3	$\left\lvert\frac{\partial h}{\partial T}\right\rvert \frac{\Delta T}{h}$	0.014
Quadratic sum				0.056

Table 7: Uncertainties on the amplitude of the calibration signal at 2f from the R4-01 rotor simple model geometry.

6 Design of a counterweight

One of the challenge of the NCal is to be able to produce a reliable system. This mainly concerns the rotors and ball bearings for a 24/7 use. To increase the reliability of the system we balance the rotor to minimize the vibrations.

To measure the slight asymmetry of the rotor we take advantage of the low resonance frequency of the NCal suspension. We measure the recoil displacement using the position sensors on the reference plate. These measurements are made at a fixed frequency of 14 Hz which is away from suspension resonances. Before any balancing we measured an amplitude of 13 μm. This value revealed that the center of gravity of the rotor was not centered on the axis. This section shows the method used to correct this unbalance and the results after a correction using a counterweight mounted on the rotor.

6.1 The circular plate on the rotor

A circular metal plate was originally designed to be mounted on the central part of the rotor (figure 6) with a hole so that a photodiode allows us to compute the frequency of the rotor. This plate is fixed on the rotor using four metal screws. The geometry of the screw holes on the rotor is shown on figure 7, considering the cartesian coordinate system the angle from each screw to the horizontal axis x is $\theta = 30°$.

To counterbalance the rotor during its rotation, an open angle counterweight can replace the circular plate to correct the center of gravity back to the axis.

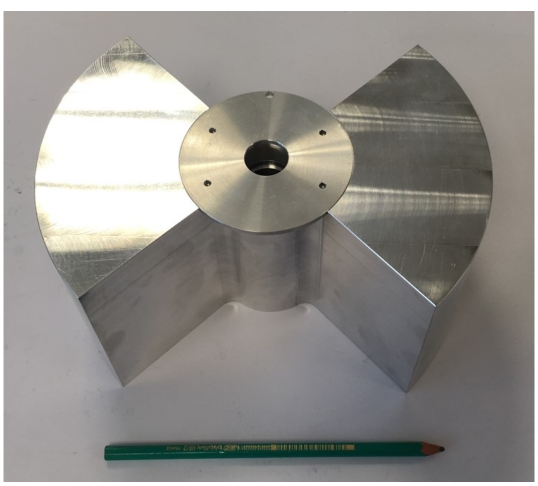

Figure 6: Circular metal plate layed on the up face of the rotor with four screw holes and the photodiode hole visible.

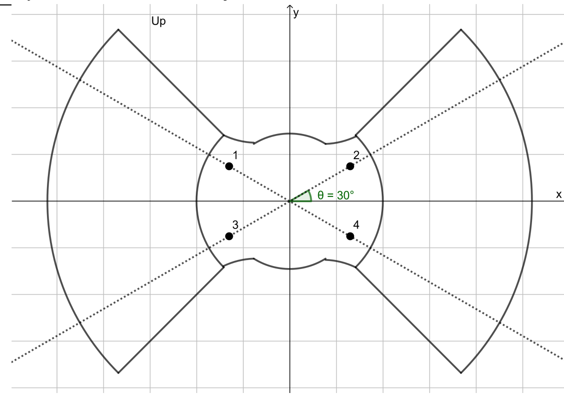

Figure 7: Representation of the up face of the rotor with the screw holes labelled from 1 to 4 and the polar angle θ.

In this part we will discuss of a semi circular aluminum plate machined as a preliminary counterweight to determine the correction to apply on the rotor.

6.2 Preliminary counterweight

6.2.1 Design of a preliminary counterweight

A semi circular plate has been machined with screw holes every 15° as shown in figure 8, this small angle incrementation would allow us to make different tests with the counterweight placed at different angles on the rotor.

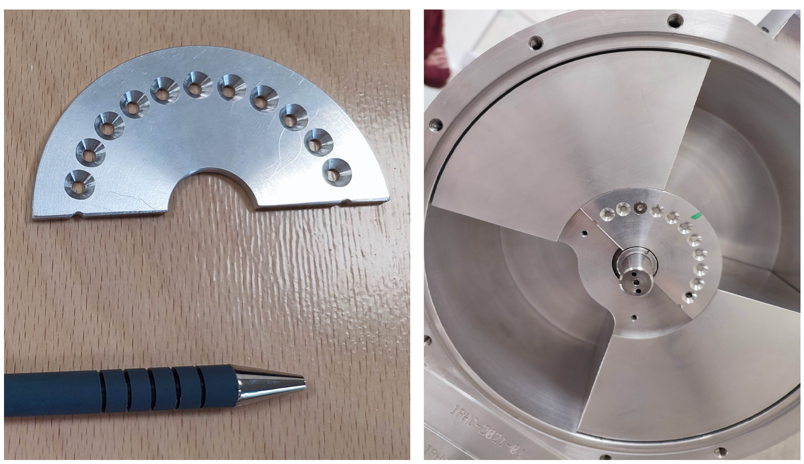

Figure 8: Left is the aluminum counterweight used with screw holes incremented every 15°. Right is the same counterweight mounted on the rotor.

6.2.2 Model of the center of gravity using moments

To correct the center of gravity of the rotor we use an analytical model considering the moment $\mathcal{M}_1$ of the counterweight and the moment $\mathcal{M}_2$ of the rotor.

Using the equation of the moment $\mathcal{M}$ where m is the mass of the object and d is the distance of the object from the axis:

$$\mathcal{M} = md \tag{7}$$

and the figure 9, we can compute the center of gravity of the two objects system (rotor and counterweight).

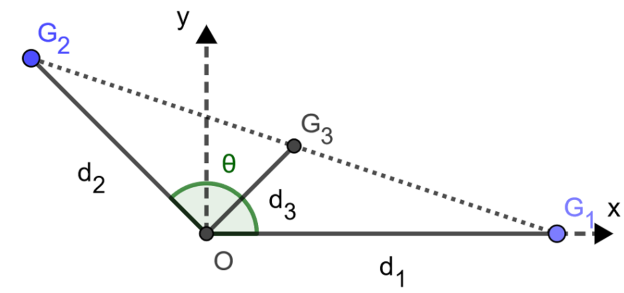

Figure 9: Representation of the center of gravity G_3 of a system composed of two objects 1 and 2 with their respective center of gravity G_1 and G_2 from the point O.

The distance d_1 is the center of gravity of the counterweight that can be set to 1 for the model. The distance d_2 is the center of gravity of the rotor equal to the ratio of the moments $\mathcal{M}_2$ and $\mathcal{M}_1$. The distance d_3 is the center of gravity of the system and can be computed using the polar angle θ and the distance d_2.
We have the following cartesian coordinates $G_i(x, y)$ for the center of gravity of each object:

$G_1(d_1, 0) = G_1(1, 0)$

$G_2(d_2 \cos\theta, d_2 \sin\theta) = G_2\left(\frac{\mathcal{M}_2}{\mathcal{M}_1}\cos\theta, \frac{\mathcal{M}_2}{\mathcal{M}_1}\sin\theta\right)$

$G_3\left(\frac{1 + d_2\cos\theta}{2}, \frac{d_2\sin\theta}{2}\right) = G_3\left(\frac{1 + \frac{\mathcal{M}_2}{\mathcal{M}_1}\cos\theta}{2}, \frac{\frac{\mathcal{M}_2}{\mathcal{M}_1}\sin\theta}{2}\right)$

finally the distance $d_3 = \sqrt{x^2 + y^2}$ can be computed:

$$d_3 = \sqrt{\frac{1}{4} + \frac{\mathcal{M}_2^2}{4\mathcal{M}_1^2} + \frac{\mathcal{M}_2}{2\mathcal{M}_1}\cos\theta} \tag{8}$$

6.3 Data taking from the position sensors

We collect the amplitude of the NCal support recoil motion when the NCal was rotating at 14 Hz. The counterweight should then give, depending on the mounting angle, a displacement greater or lower than the 13 μm obtained with the rotor without counterweight.

The figure 10 shows this amplitude as a function of the mounting angle of the counterweight on the rotor. The black dotted points represent the data from the motion sensors, the red line is a fit on the data using the model from equation 8 and the blue line is the same model assuming the ratio between $\mathcal{M}_2$ and $\mathcal{M}_1$ is equal to 1 (i.e a counterweight with the correct moment but with different mounting angles).

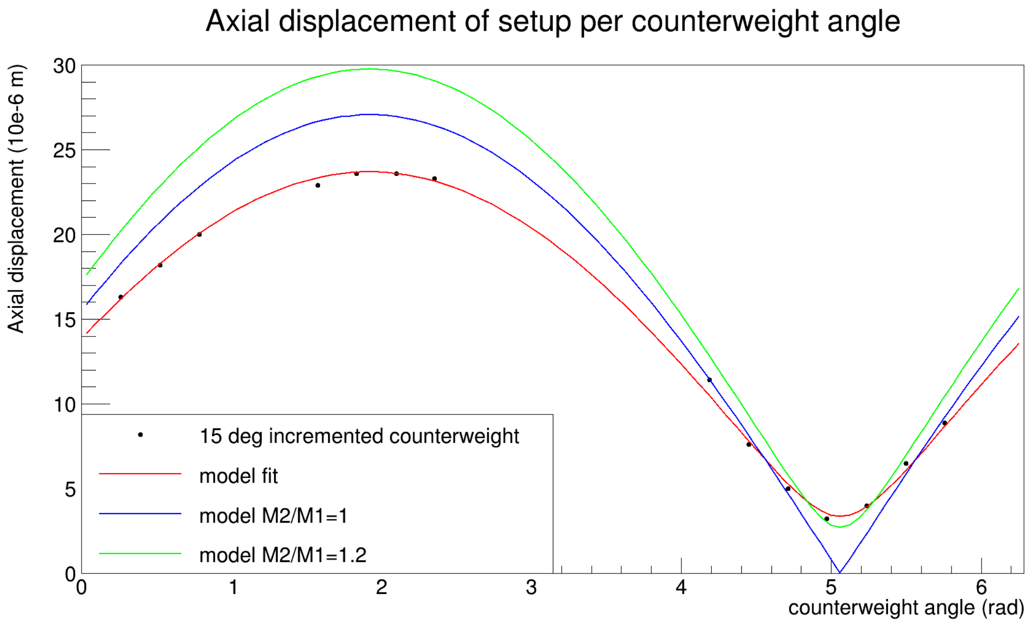

Figure 10: Amplitude of the axial displacement as a function of the angle of the counterweight. Data is shown as black dots, then fitted using the model in red, the blue line shows the model assuming the ratio between moments $\mathcal{M}_1$ and $\mathcal{M}_2$ is equal to 1, the green line shows the model assuming the moments ratio is 1.2.

The blue line gives the minimum displacement of 0 μm for an angle of 5.06 rad or 289.9°. This angle is therefore where the counterweight should be placed to compensate the moment of the unbalanced rotor. The green line represents the moments ratio equal to 1.2, this shows that in our case the ratio is below 1.

We have to note that the number of screws used was not always the same and their position neither, meaning that the data taking is a bit less precise than if all four screws were used for every measure. This issue has to be taken into account as the correction gets more precise.

6.4 Counterweight tuning

In this section we will discuss about the making of a stainless steel counterweight using the results from last section.

6.4.1 Machined circular plate

The purpose of a stainless steel counterweight is that the higher density of the material makes the counterweight more massive for the same dimensions to limit the material to be removed from the counterweight and keep enough screw/holes. In a first place, a circular plate is machined as shown in figure 11.

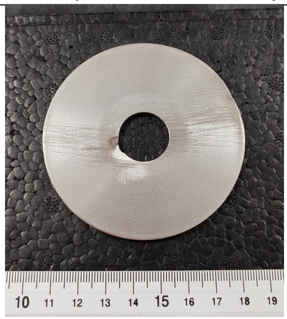

Figure 11: Machined circular stainless steel plate.

It is designed to be the same inner and outer radius as the aluminum plate (10 mm and 40 mm).

6.4.2 Determination of the geometry of the counterweight

From figure 10 the model fit gave $\mathcal{M}_2/\mathcal{M}_1 = 0.75$ while the targetted result is $\mathcal{M}_2/\mathcal{M}_1 = 1$ so we must have $\mathcal{M}_1 = \mathcal{M}_2 = m\, d_1/0.75 = 3.63 \times 10^{-4}$ kg.m (m being the required mass for the counterweight and d_1 its center of gravity). Assuming the center of gravity of the counterweight would be the following:

$$d = \frac{\rho}{m} \int_r^R \int_0^\theta \int_0^h r\mathrm{d}V \tag{9}$$

with the parameters:

$\rho = 7776$ kg.m^{-3}

$r = 10.04 \times 10^{-3}$ m and $R = 39.95 \times 10^{-3}$ m

$h = 2.00 \times 10^{-3}$

These are the mean values of each measured parameter, stainless steel is harder to machine than aluminum therefore the dimensions are less precise.

Now we have this equation for $\mathcal{M}_1$:

$$\mathcal{M}_1 = dm = \rho \iiint r\mathrm{d}V = 3.63 \times 10^{-4} \text{ kg.m} \tag{10}$$

By computing eq. (10) we find $\theta = 64.04°$, resulting in the geometry shown in figure 12.

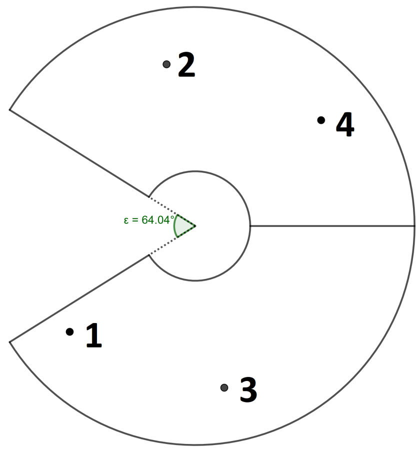

Figure 12: Geometry of the stainless steel counterweight to be machined. The computed opening angle has a value of 64.04°. Screw holes are labelled from 1 to 4.

6.4.3 Testing the theoretical geometry

Now that the theoretical geometry has been determined, we have to test the machined counterweight and check if any adjustment is necessary.

The tests shown that the geometry gave a lower axial displacement value than the minimum of the data from figure 10 with values between 2.0 μm and 2.9 μm depending on the location of the screws. The fact that the results did not give a value of displacement closer to zero can be explained by:

- The number and placement of the screws was not taken into account during the preliminary tests making the measures slightly uneven (a screw weighs below 1 g).
- The theoretical model does not include screw holes.
- The stainless steel plate was roughly machined, the thickness and diameter values were averaged to mean values.

A further correction is therefore needed to achieve a lower axial displacement.

6.4.4 Final corrections on the counterweight

During further tests we noticed that the residual recoil motion was less than 0.4 μm with a configuration of one large screw and eight nuts on hole 4 and one medium screw and one nut on hole 3 (the screw holes are the ones labelled on figure 10). Weighing the screws and nuts revealed that we needed to remove material equal to 4.1 g of material on the opposite of hole 4 (hole 1) and 1.5 g of material on the opposite of hole 3 (hole 2).

Considering the actual geometry of the counterweight shown on figure 12 we reduced the material on the counterweight as shown on figure 13. Since the quantity of material needed to be removed is larger on hole 1 than hole 2, the shape of the cuts are very different (one section of disk is removed on hole 1 while only a small external layer is removed above hole 2 on figure 13).

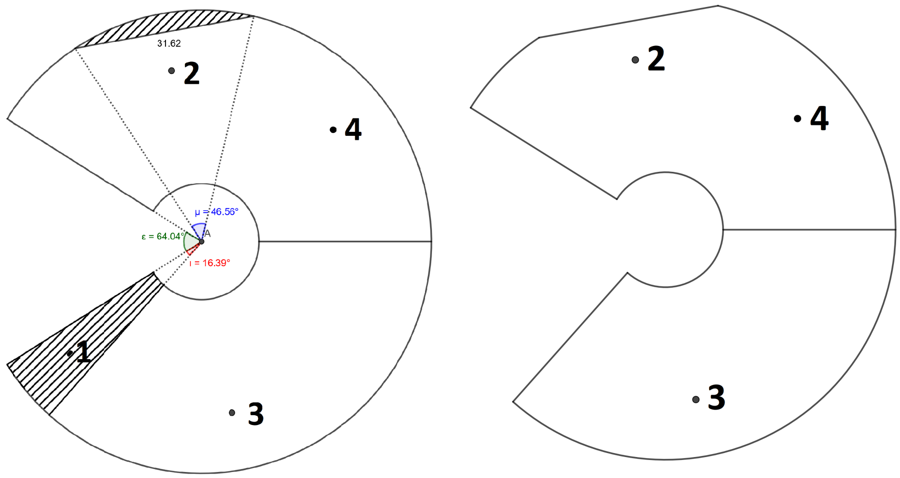

Figure 13: Final geometry of the counterweight with trimmed material located on screw hole 1 and next to hole 2. Left is the geometry of the counterweight with the cuts displayed as hatched areas, right is the remaining material on the counterweight after the cuts.

This last counterweight geometry was tested and resulted in a recoil motion of 0.2 μm using four small screws. We consider this value to be acceptable for the balancing of the rotor.

7 Characterization of the rotor using an advanced model

7.1 Thickness

A more advanced model can be used considering the deformations on the surfaces of the sectors for better accuracy. Each measurement point of table 4 can be considered as a sub-sector with its own thickness.

The uncertainty on this value is more complex to evaluate. As a conservative approach we use the maximum rms of the deviation to a plane for both sector (8.3 μm see section 4.1) to which we add linearly the uncertainty on the flatness of the measurement table (2.0 μm) as well as the measurement tool (2.2 μm). The total uncertainty on the thickness is 13 μm.

7.2 Radius

On figure 3 we divided the external sectors in 4 sub-sectors for each sector (blue points). We convert the point of table 6 to the grid of figure 3 by averaging the two closest values and converting them to 23°C. The results are shown in table 8. We notice that the R sector is on average 9 μm larger than the L sector.

Radius	L sector		R sector	
	Up	Down	Up	Down
1	104.024	104.024	104.036	104.037
2	104.039	104.037	104.044	104.044
3	104.039	104.037	104.044	104.044
4	104.024	104.024	104.036	104.037

Table 8: Radius measurements (in mm at 23°C) for the L and R sectors of R4-01.

The maximum rms of the radii for both sector is 7.4 μm. The tool uncertainty is 2.4 μm. Like for the thickness we use a linear sum and find the uncertainty on both radii to be 10 μm.

7.3 Chamfers on the rotor

The rotor has been machined with four chamfers on the inner radius as shown on figure 14 (see drawing at the end of the note). Adding the chamfers to the geometry is expected to lower the 2f signal. This effect will be studied using FROMAGE.

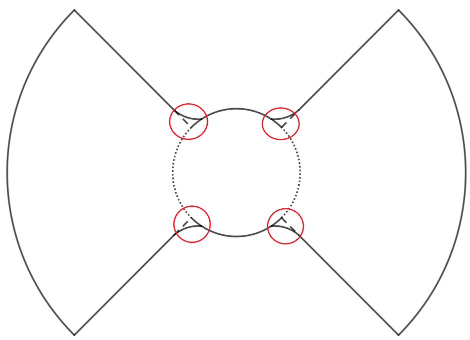

Figure 14: Outline of the rotor with the chamfers circled in red.

7.4 Opening angles and asymmetry

The opening angles of the full and empty sectors have been measured using a video microscope. We measured two points on each side of the sectors and then we computed the angle between each line using the microscope interface.

7.4.1 Uncertainty

The uncertainty of the video microscope is 2 μm. To determine the uncertainty on the opening angle we will consider the method described by fig. 15.

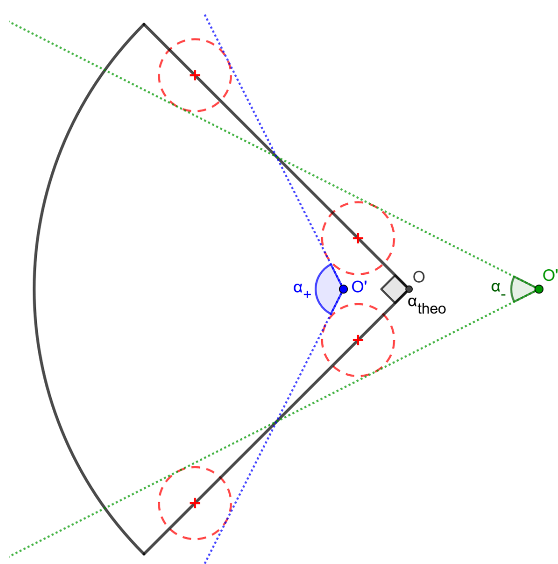

Figure 15: Method used to determine the uncertainty on the opening angles using the video microscope. In red are shown the points used to determine the two lines for the opening angle computation, the red dotted circles represent their uncertainty ($\pm$ 2 μm). The theoretical angle α_{theo} is equal to $\pi/2$, α_+ and α_- are the maximum and minimum values of the error on this angle. The proportions have been amplified for the visualization. This method combines the uncertainties in the most pessimistic way making them conservative.

Using this method we found the uncertainty on the angle α and the asymmetry Ψ to be $(\alpha_+ - \alpha_-)/2 =$ 0.2 mrad. In the 2f signal computation the opening angle contributes as $\sin(\alpha)$, the error propagates as $\delta\alpha^2 \sin(\alpha)$ giving an uncertainty of 4×10^{-6} % which is neglectable. The asymmetry contributes as $\cos(2\Psi)$ which propagates as $4\delta\Psi^2 cos(\Psi)$ giving an uncertainty of 1.6×10^{-5} % which is also neglectable.

7.4.2 Measurements

Since the opening angles are independant of the temperature the values are the same at 23°C. The measurements are shown in table 9. The mean value is associated to the center value. And the difference between the up and down values is shown.

Opening angle	Up	Down	Mean	Difference
L	1.57105	1.57231	1.57168	-0.00126
R	1.57095	1.57281	1.57188	-0.00186
L-R	1.57058	1.56939	1.56998	0.00120
R-L	1.57059	1.56868	1.56964	0.00192

Table 9: Opening angle measurements in rad for the L, R full sectors and L-R, R-L empty sectors of R4-01.

These measurements allow us to compute the signal with different opening angles and an asymetry between the sectors. They will be included in the advanced model described in the next section. The asymmetry offset between the L and R sector can be computed with a sum of L-R, L/2 and R/2 angles which gives an offset of 0.2 mrad compared to the theoretical value of π.

However, the offsets of the angles computed in table 9 as well as the asymetry compared to the theoretical value are of the same order than their associated uncertainty of 0.2 mrad so the 2f signal should not be impacted.

7.5 Expected NCal signals and uncertainties

7.5.1 Advanced model including chamfers and counterweight

The geometry used to describe the rotor as an advanced model is represented in figure 16. The external part of the sectors are divided in 2 sub-sectors each to correspond to the different radii determined. In addition we include the counterweight, the screws, the screw holes, the opening angles and asymmetry of the sectors.

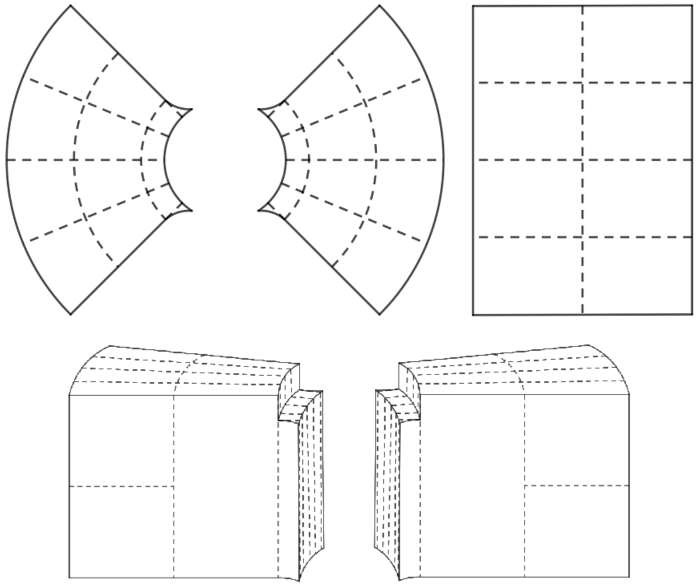

Figure 16: Advanced model geometry used to describe the rotor. Top left is a front view, top right is a side view (external sub-sectors) and bottom is a tilted view of the sectors. Only the 4 external part sectors are divided in 2 sub-sectors each. The chamfers are visible on the inner radius.

Using FROMAGE on this full geometry gives the following strains:

- strain(1f) $= \dfrac{8.4584 \times 10^{-20}}{(1f_{rot})^2}$
- strain(2f) $= \dfrac{2.1207 \times 10^{-18}}{(2f_{rot})^2}$
- strain(3f) $= \dfrac{2.4881 \times 10^{-23}}{(3f_{rot})^2}$

We can use FROMAGE to create files containing the position of each element to display them as shown on figure 17 (the grid used for the computation is the same as the one used for these images: 16x65x40 for the rotor and counterweight).

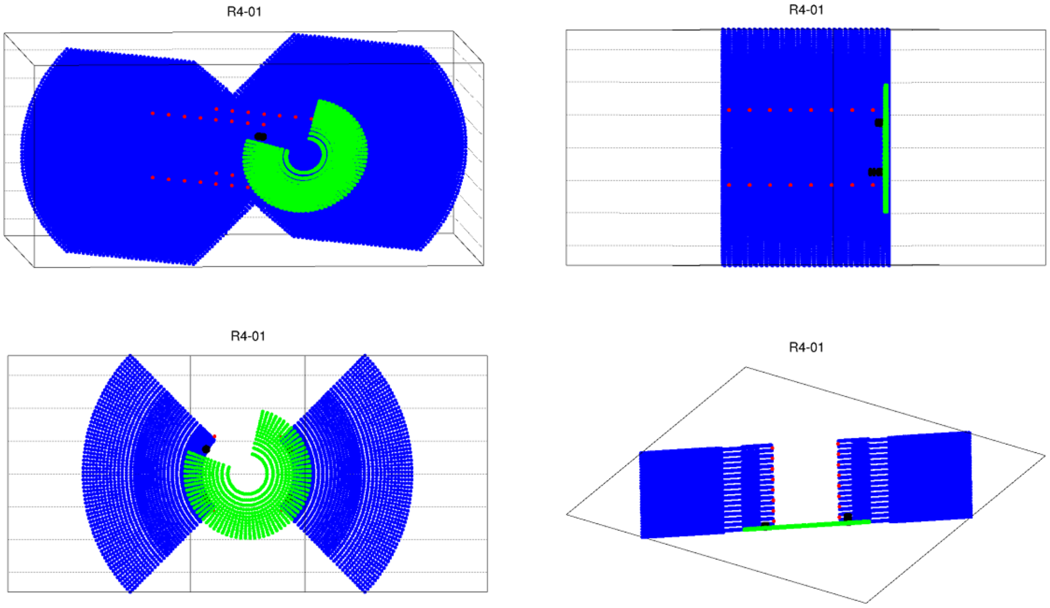

Figure 17: Cloud of points views of the position of each rotor and counterweight element from FROMAGE. Top left is a general view, top right is a side view, bottom left is a front view and bottom right is an upper view. The rotor sectors are shown in blue, the counterweight in green, the chamfers in red and the screws in black.

7.5.2 Chamfers effect

Removing the chamfers from the advanced model we obtain the following strains:

- strain(1f) $= \dfrac{8.4587 \times 10^{-20}}{(1f_{rot})^2}$
- strain(2f) $= \dfrac{2.1209 \times 10^{-18}}{(2f_{rot})^2}$
- strain(3f) $= \dfrac{2.4876 \times 10^{-23}}{(3f_{rot})^2}$

The relative deviations from the advanced model of section 7.5.1 are:

- (1f) : 0.004%
- (2f) : 0.009%
- (3f) : 0.020%

The chamfers have a larger impact on the 3f than the 1f and 2f strain signals. The 1f and 2f signals decrease with the presence of chamfers while the 3f signal increases. In the advanced model it is expected that the counterweight compensates some of the 1f signal from the chamfers so this geometry might not be complete.

7.5.3 Counterweight effects using FROMAGE

Using FROMAGE we can compute the gravitationnal effect of the counterweight mounted on the rotor. We note that four screws were used to mount the counterweight on the rotor and have to be taken into account.

Table 10 shows the effects of each element considered on the advanced rotor model (without chamfers).

Geometry	strain/(1f)^2	strain/(2f)^2	strain/(3f)^2
rotor	5.9110×10^{-21}	2.1202×10^{-18}	1.2538×10^{-23}
rotor + screw holes	5.9110×10^{-21}	2.1202×10^{-18}	1.2538×10^{-23}
rotor + counterweight (w.o screws)	8.4586×10^{-20}	2.1208×10^{-18}	2.4876×10^{-23}
rotor + counterweight (w. screws)	8.4587×10^{-20}	2.1209×10^{-18}	2.4876×10^{-23}

Table 10: Strain up to 3f for additionnal geometries of R4-01.

The screw holes and screws have an effect below the grid uncertainty of FROMAGE (0.005% on 2f) and can be neglected in the 2f signal.

The presence of the counterweight (w. screws) induces the following relative deviations from the rotor without counterweight:

- σ(1f) = 30.1%
- σ(2f) = 0.033%
- σ(3f) = 9.4%

The relative deviations on 1f and 3f are very large compared to the counterweight effect on the 2f signal. The counterweight increases the 1f signal, this geometry might therefore not be complete.

7.5.4 Remaining geometry uncertainty

After considering every elements of the rotor geometry, the 1f signal is still significant while the rotor has been balanced. This indicates that the geometry is not perfectly known.

It is also the rotor that requires the largest counterweight. This is likely due to a different machining of the sectors (see fig. 18) since rotor R4-02 and following were machined in a single day (unlike R4-01 which was machined in two days), they also benefit of a larger number of pass with reduced thickness that produces a better side surface.

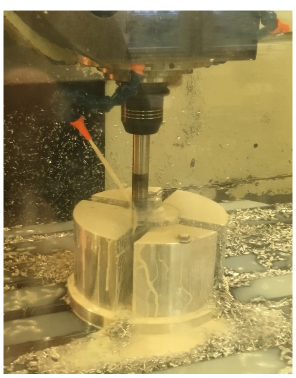

Figure 18: Machining of the sides of the rotor.

For a better understanding of the rotor geometry, we measured the sides of each rotor with the microscope to determine the center of each face of each sector compared to the axis center O (see fig. 19). We notice that there is around 0.2 mm of offset between the center of each sector and the axis center. The offsets are also different face up to face down.

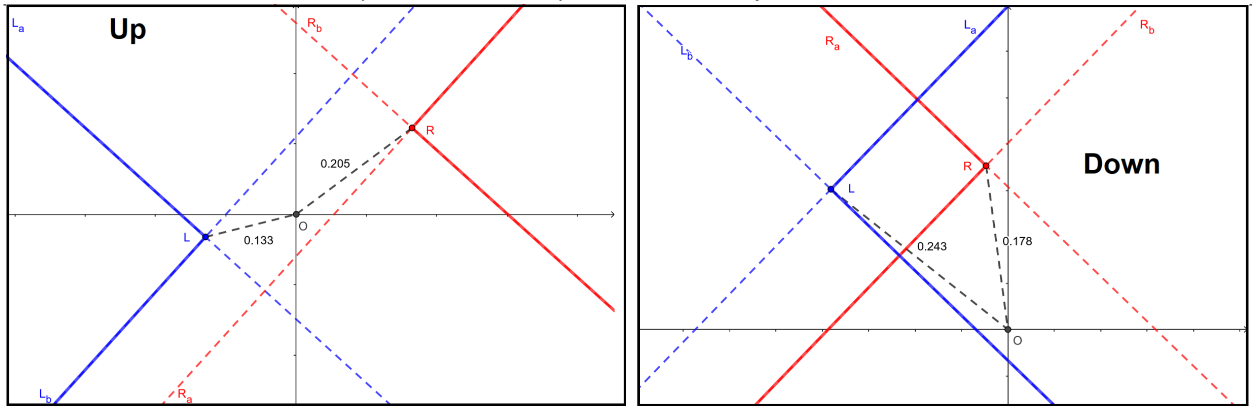

Figure 19: Offset of the centers of the centers to the axis center in mm. Left is face up, right is face down. L sector is shown in blue and R sector in red.

In FROMAGE we add thin blocks of positive or negative mass to model the offsets. The thickness ϵ of the blocks is shown in table 11 corresponding to the axis offsets shown in fig. 19:

Side	Up thickness ϵ	Down thickness ϵ
L_a	(-) 111	(+) 242
L_b	(-) 74	(+) 24
R_a	(-) 40	(+) 111
R_b	(-) 201	(-) 139

Table 11: Thickness ϵ (in μm) of the positive/negative mass blocks added in FROMAGE. The sign (+) corresponds to a positive mass and (-) to a negative mass. The remaining dimensions of the blocks correspond to their associated sub-sector.

Using this configuration (displayed in Appendix A) we obtain the following 1f and 2f strains:

- strain(1f) $= \dfrac{1.9391 \times 10^{-20}}{(1f_{rot})^2}$
- strain(2f) $= \dfrac{2.1207 \times 10^{-18}}{(2f_{rot})^2}$

In this geometry the counterweight reduces the 1f signal by a factor 4.3 while the 2f signal remains the same as in section 7.5.1. We can consider an opening angle and sector asymmetry uncertainty on the 2f signal, the value is therefore $<5 \times 10^{-4}$ %.

We can reduce the 1f by adjusting the ϵ parameter. Using L_a = 5 μm and L_b = 150 μm on the up face we find a 1f signal of $1.1916 \times 10^{-21}/(1f)^2$ reduced by a factor 16.2, the 2f signal remains the same, the remaining geometry uncertainty is therefore $<5 \times 10^{-4}$ %.

This confirms the weak sensitivity to the exact position/shape of the flat surfaces defining the sectors.

7.5.5 Uncertainties

To set an uncertainty on the strain(2f) from the description of the geometry we take the difference between the simple model (strain(2f) $= 2.1210 \times 10^{-18}/(2f)^2$) and the advanced model (strain(2f) $= 2.1207 \times 10^{-18}/(2f)^2$). This deviation, 0.014%, is reported in table 12 as modelling uncertainty.

The uncertainties considered for this full model are displayed in table 12.

R4-01 rotor parameter advanced model (23°C)			NCal 2f signal uncertainty	
name	mean value	uncertainty	formula	value (%)
Density ρ (kg.m^{-3})	2808.1	0.2	$\delta\rho/\rho$	0.007
Thickness b left sector (12 sub-sectors) (mm) Thickness b right sector (12 sub-sectors) (mm)	104.322 104.307	1.3×10^{-2}	$\delta b/b$	0.012
r_{max} left sector (8 ext sub-sectors) (mm) r_{max} right sector (8 ext sub-sectors) (mm)	104.031 104.040	1.0×10^{-2}	$4\delta r_{max}/r_{max}$	0.037
G (m^3.kg^{-1}.s^{-2})	$6.674\,30 \times 10^{-11}$	1.5×10^{-15}	$\delta G/G$	0.002
Temperature T (°C)	23	3	$\left\|\frac{\partial h}{\partial T}\right\| \frac{\Delta T}{h}$	0.014
Modelling Uncertainty				0.014
FROMAGE grid uncertainty				0.005
Opening angle and sector asymmetry uncertainty				$<5 \times 10^{-4}$
Remaining geometry uncertainty				$<5 \times 10^{-4}$
Total uncertainty from the rotor (quadratic sum)				0.045

Table 12: Uncertainties on the amplitude of the calibration signal at 2f from the R4-01 rotor advanced model geometry at 23°C.

A Appendix

```
### This is a cfg file for a more realistic geometry of the mirror and the Virgo NCal R4-01 (2022)

### ALL THE OBJECTS ARE DEFINED IN THE MIRROR'S FRAME (O,x,y,z),
### with O the center of the mirror, x axis along the ITF's beam toward the beam-splitter,
### y axis orthogonal to x in the plane of the ITF,
### z axis orthogonal to the plane of the ITF upward

### MIRROR DEFINITION

GRID_SIZE 12 30 8

CYLINDER 2202. 0 0.175 0.2 360 0 0 0

GRID_SIZE 1 1 1

# Defining the flats on the edge of the mirror
CUT_CYL 2202. 0.175 0.2 0.05 0 0
CUT_CYL 2202. 0.175 0.2 0.05 0 180

# Defining the ears and anchors of the mirror
CUBOID 2202. 0.090 0.010 0.015  0     0.1782 -0.0125
CUBOID 2202. 0.090 0.010 0.015  0    -0.1782 -0.0125
CUBOID 2202. 0.039 0.008 0.008 -0.02 -0.1772 -0.024
CUBOID 2202. 0.039 0.008 0.008 -0.02  0.1772 -0.024
CUBOID 2202. 0.039 0.008 0.008  0.02 -0.1772 -0.024
CUBOID 2202. 0.039 0.008 0.008  0.02  0.1772 -0.024

### ROTOR DEFINITION: CYLINDER DENSITY INNER_RADIUS OUTER_RADIUS THICKNESS OPEN_ANGLE r z theta
ROTOR_CYLINDRICAL 1.7 34.7 0 0

## COUNTERWEIGHT 7776.
GRID_SIZE 16 65 40
CYLINDER 7776. 0.01004 0.03995 0.00200 279.57 0 0.048594 298.085
GRID_SIZE 1 1 1
CUT_CYL 7776. 0.03995 0.00200 0.03162 0.048594 30

## SCREW HOLES
GRID_SIZE 1 1 1
CYLINDER -2808.1 0 0.0015 0.012 360 0.03 0.04463796542518 150
CYLINDER -2808.1 0 0.0015 0.012 360 0.03 0.04462946484344 30
CYLINDER -2808.1 0 0.0015 0.012 360 0.03 0.04463446518564 210
CYLINDER -2808.1 0 0.0015 0.012 360 0.03 0.04462746470656 330

CYLINDER -7776. 0 0.0015 0.002 360 0.03 0.0485940071109 30
CYLINDER -7776. 0 0.0015 0.002 360 0.03 0.0485940071109 210
CYLINDER -7776. 0 0.0015 0.002 360 0.03 0.0485940071109 330

## SCREWS COUNTERWEIGHT
GRID_SIZE 1 1 1
CYLINDER 7600. 0 0.0015 0.00945 360 0.03 0.04285955031798 150
CYLINDER 7600. 0 0.0015 0.00945 360 0.03 0.04385955031798 30
CYLINDER 7600. 0 0.0015 0.00945 360 0.03 0.04385955031798 210
CYLINDER 7600. 0 0.0015 0.00945 360 0.03 0.04385955031798 330
```

```
# VERY FAST
#GRID_SIZE 4 4 4
# FAST
#GRID_SIZE 8 17 14
# SLOW
GRID_SIZE 8 65 40

## L sector
## Up face
## Inner part
OUTER_FILLET 2808.1 0.02893 0.05063796542518 0.02227502439834 0.01 -11.2518 146.2446
CYLINDER 2808.1 0.02893 0.03999 0.05063796542518 22.5036 0 0.02227502439834 146.2446
CYLINDER 2808.1 0.02893 0.03999 0.05063446518564 22.5036 0 0.02226627379949 168.7482
CYLINDER 2808.1 0.02893 0.03999 0.05063196501454 22.5036 0 0.02227202419302 191.2518
CYLINDER 2808.1 0.02893 0.03999 0.05062946484344 22.5036 0 0.02227077410747 213.7554
OUTER_FILLET 2808.1 0.02893 0.05062946484344 0.02227077410747 0.01 11.2518 213.7554

## Middle part
CYLINDER 2808.1 0.03999 0.071989 0.0521660700015 22.5036 0 0.02608303500075 146.2446
CYLINDER 2808.1 0.03999 0.071989 0.05216056962508 22.5036 0 0.02608028481254 168.7482
CYLINDER 2808.1 0.03999 0.071989 0.05215756941976 22.5036 0 0.02607878470988 191.2518
CYLINDER 2808.1 0.03999 0.071989 0.05215556928288 22.5036 0 0.02607778464144 213.7554

## Outer part
CYLINDER 2808.1 0.071989 0.104024 0.0521730885408957 22.5036 0 0.0260865442704478 146.2446
CYLINDER 2808.1 0.071989 0.104039 0.052168593887535 22.5036 0 0.0260842969437675 168.7482
CYLINDER 2808.1 0.071989 0.104039 0.0521586622713485 22.5036 0 0.0260793311356743 191.2518
CYLINDER 2808.1 0.071989 0.104024 0.0521482331132829 22.5036 0 0.0260741165566414 213.7554

## Down face
## Inner part
OUTER_FILLET 2808.1 0.02893 0.05063796542518 -0.02227502439834 0.01 -11.2608 146.2175
CYLINDER 2808.1 0.02893 0.03999 0.05063796542518 22.5217 0 -0.02227502439834 146.2175
CYLINDER 2808.1 0.02893 0.03999 0.05063446518564 22.5217 0 -0.02226627379949 168.7392
CYLINDER 2808.1 0.02893 0.03999 0.05063196501454 22.5217 0 -0.02227202419302 191.2608
CYLINDER 2808.1 0.02893 0.03999 0.05062946484344 22.5217 0 -0.02227077410747 213.7825
OUTER_FILLET 2808.1 0.02893 0.05062946484344 -0.02227077410747 0.01 11.2608 213.7825

## Middle part
CYLINDER 2808.1 0.03999 0.071989 0.0521660700015 22.5217 0 -0.02608303500075 146.2175
CYLINDER 2808.1 0.03999 0.071989 0.05216056962508 22.5217 0 -0.02608028481254 168.7392
CYLINDER 2808.1 0.03999 0.071989 0.05215756941976 22.5217 0 -0.02607878470988 191.2608
CYLINDER 2808.1 0.03999 0.071989 0.05215556928288 22.5217 0 -0.02607778464144 213.7825

## Outer part
CYLINDER 2808.1 0.071989 0.104024 0.0521730885408957 22.5217 0 -0.0260865442704478 146.2175
CYLINDER 2808.1 0.071989 0.104037 0.052168593887535 22.5217 0 -0.0260842969437675 168.7392
CYLINDER 2808.1 0.071989 0.104037 0.0521586622713485 22.5217 0 -0.0260793311356743 191.2608
CYLINDER 2808.1 0.071989 0.104024 0.0521482331132829 22.5217 0 -0.0260741165566414 213.7825

## R sector
## Up face
## Inner part
OUTER_FILLET 2808.1 0.02893 0.05063446518564 0.0222778184437777 0.01 11.2511 33.7435
CYLINDER 2808.1 0.02893 0.03999 0.05063446518564 22.5022 0 0.0222778184437777 33.7435
CYLINDER 2808.1 0.02893 0.03999 0.05063146498032 22.5022 0 0.0222703179304777 11.2412
```

```
CYLINDER 2808.1 0.02893 0.03999 0.05062896480922 22.5022 0 0.0222640675027277 348.7390
CYLINDER 2808.1 0.02893 0.03999 0.05062746470656 22.5022 0 0.0222603172460777 326.2368
OUTER_FILLET 2808.1 0.02893 0.05062746470656 0.0222603172460777 0.01 -11.2511 326.2368

## Middle part
CYLINDER 2808.1 0.03999 0.071989 0.05216056962508 22.5022 0 0.02608028481254 33.7435
CYLINDER 2808.1 0.03999 0.071989 0.0521572956866379 22.5022 0 0.0260786478433189 11.2412
CYLINDER 2808.1 0.03999 0.071989 0.0521512972664239 22.5022 0 0.026075648633212 348.7390
CYLINDER 2808.1 0.03999 0.071989 0.0521475264625028 22.5022 0 0.0260737632312514 326.2368

## Outer part
CYLINDER 2808.1 0.071989 0.104036 0.0521665319785161 22.5022 0 0.0260832659892581 33.7435
CYLINDER 2808.1 0.071989 0.104044 0.0521561028204504 22.5022 0 0.0260780514102252 11.2412
CYLINDER 2808.1 0.071989 0.104044 0.0521471712727039 22.5022 0 0.026073585636352 348.7390
CYLINDER 2808.1 0.071989 0.104036 0.0521406764824633 22.5022 0 0.0260703382412316 326.2368

## Down face
## Inner part
OUTER_FILLET 2808.1 0.02893 0.05063446518564 -0.0222778184437777 0.01 11.2644 33.7835
CYLINDER 2808.1 0.02893 0.03999 0.05063446518564 22.5289 0 -0.0222778184437777 33.7835
CYLINDER 2808.1 0.02893 0.03999 0.05063146498032 22.5289 0 -0.0222703179304777 11.2546
CYLINDER 2808.1 0.02893 0.03999 0.05062896480922 22.5289 0 -0.0222640675027277 348.7257
CYLINDER 2808.1 0.02893 0.03999 0.05062746470656 22.5289 0 -0.0222603172460777 326.1968
OUTER_FILLET 2808.1 0.02893 0.05062746470656 -0.0222603172460777 0.01 -11.2644 326.1968

## Middle part
CYLINDER 2808.1 0.03999 0.071989 0.05216056962508 22.5289 0 -0.02608028481254 33.7835
CYLINDER 2808.1 0.03999 0.071989 0.0521572956866379 22.5289 0 -0.0260786478433189 11.2546
CYLINDER 2808.1 0.03999 0.071989 0.0521512972664239 22.5289 0 -0.026075648633212 348.7257
CYLINDER 2808.1 0.03999 0.071989 0.0521475264625028 22.5289 0 -0.0260737632312514 326.1968

## Outer part
CYLINDER 2808.1 0.071989 0.104037 0.0521665319785161 22.5289 0 -0.0260832659892581 33.7835
CYLINDER 2808.1 0.071989 0.104044 0.0521561028204504 22.5289 0 -0.0260780514102252 11.2546
CYLINDER 2808.1 0.071989 0.104044 0.0521471712727039 22.5289 0 -0.026073585636352 348.7257
CYLINDER 2808.1 0.071989 0.104037 0.0521406764824633 22.5289 0 -0.0260703382412316 326.1968

## CUBOIDS
GRID_SIZE 1 1 1
## L sector
## Up face
## Inner part
CUBOID -2808.1 0.05063796542518 0.01106 0.000111 0.02227502439834 -0.024403046 0.0243307
CUBOID -2808.1 0.05062946484344 0.01106 0.000074 0.02227077410747 -0.024363797 -0.024370002

## Middle part
CUBOID -2808.1 0.0521660700015 0.031999 0.000111 0.02608303500075 -0.039585687 0.039595422
CUBOID -2808.1 0.05215556928288 0.031999 0.000074 0.02607778464144 -0.039585482 -0.039595627

## Outer part
CUBOID -2808.1 0.0521660700015 0.032035 0.000111 0.0260865442704478 -0.062222452 0.062237533
CUBOID -2808.1 0.0521482331132829 0.032035 0.000074 0.0260741165566414 -0.062221946 -0.062238039

## Down face
## Inner part
CUBOID 2808.1 0.05063796542518 0.01106 0.000242 -0.02227502439834 -0.024348565 0.02438522
```

```
CUBOID 2808.1 0.05062946484344 0.01106 0.000024 -0.02227077410747 -0.024348454 -0.024385332

## Middle part
CUBOID 2808.1 0.0521660700015 0.031999 0.000242 -0.02608303500075 -0.03956087 0.039620218
CUBOID 2808.1 0.05215556928288 0.031999 0.000024 -0.02607778464144 -0.039560574 -0.039620513

## Outer part
CUBOID 2808.1 0.0521660700015 0.032035 0.000242 -0.0260865442704478 -0.062183573 0.062276378
CUBOID 2808.1 0.0521482331132829 0.032035 0.000024 -0.0260741165566414 -0.062182844 -0.062277106

## R sector
## Up face
## Inner part
CUBOID -2808.1 0.05063446518564 0.01106 0.00004 0.0222778184437777 0.024369186 0.024364613
CUBOID -2808.1 0.05062746470656 0.01106 0.000201 0.0222603172460777 0.024360899 -0.02437290

## Middle part
CUBOID -2808.1 0.05216056962508 0.031999 0.00004 0.02608028481254 0.039594253 0.039586856
CUBOID -2808.1 0.0521475264625028 0.031999 0.000201 0.0260737632312514 0.039580892 -0.039600216

## Outer part
CUBOID -2808.1 0.0521665319785161 0.032047 0.00004 0.0260832659892581 0.062240009 0.062228461
CUBOID -2808.1 0.0521406764824633 0.032047 0.000201 0.0260703382412316 0.062219246 -0.062249222

## Down face
## Inner part
CUBOID 2808.1 0.05063446518564 0.01106 0.000111 -0.0222778184437777 0.024346466 0.024387316
CUBOID -2808.1 0.05062746470656 0.01106 0.000139 -0.0222603172460777 0.024338175 -0.02439559

## Middle part
CUBOID 2808.1 0.05216056962508 0.031999 0.000111 -0.02608028481254 0.039557308 0.039623774
CUBOID -2808.1 0.0521475264625028 0.031999 0.000139 -0.0260737632312514 0.039543944 -0.039637111

## Outer part
CUBOID 2808.1 0.0521665319785161 0.032048 0.000111 -0.0260832659892581 0.062182216 0.062286918
CUBOID -2808.1 0.0521406764824633 0.032048 0.000139 -0.0260703382412316 0.062161458 -0.062307635

## GENERAL PARAMETERS

STEP 22.5 16

ARM_LENGTH 3000

SIGNAL 3
```

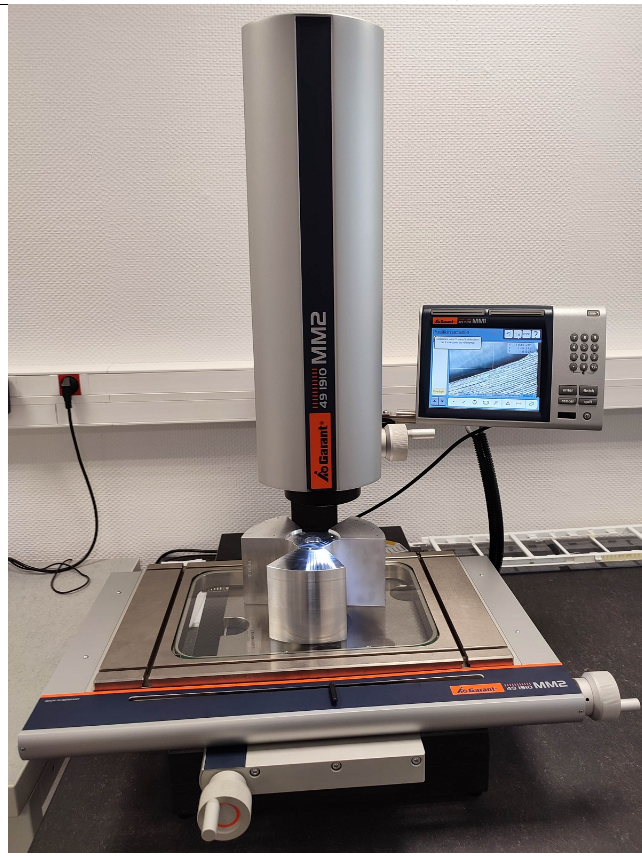

Figure 20: Video measuring microscope coupled with translation table used to determine the opening angles of the rotor. The model is a GARANT MM2.

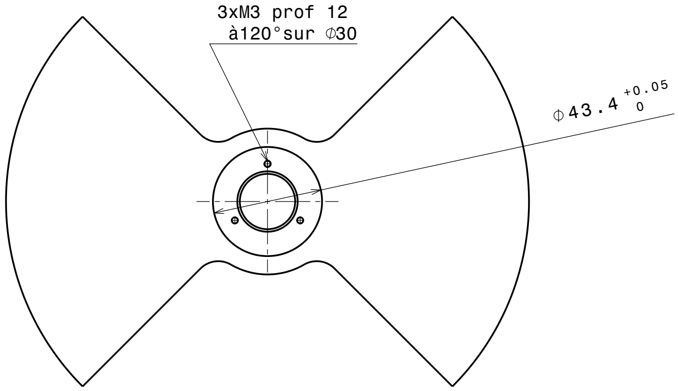

Vue derrière
Echelle : 1:2

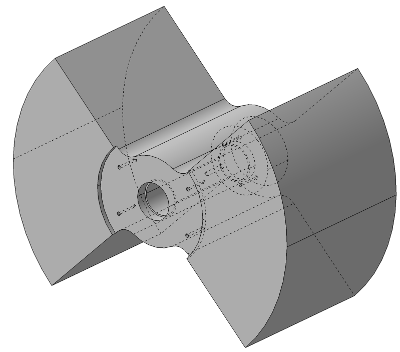

Vue isométrique
Echelle : 1:3

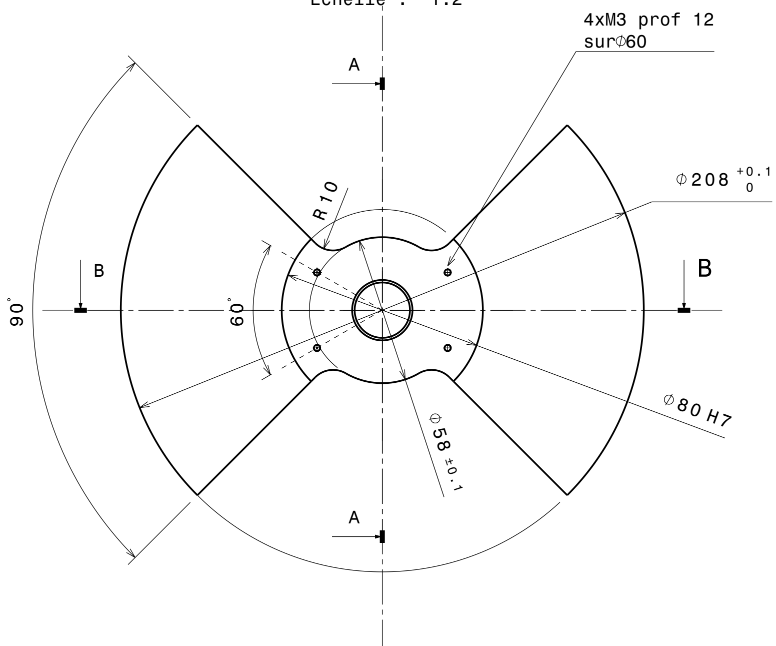

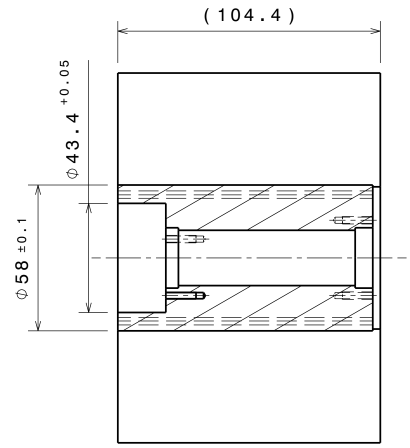

Coupe A-A
Echelle : 1:2

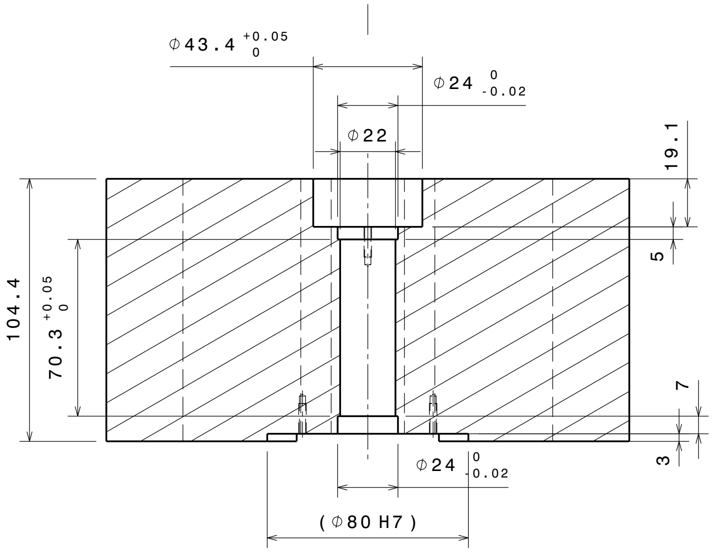

Coupe B-B
Echelle : 1:2

	1	**AW-7075**		5	
N°	Qté	Matière	Traitement de surface	Masse Kg	Dessin d'ensemble
Rug. gén. : **Ra = 1,6**		Tol. gén. : **ISO 2768 mK**	Chanfreins: **0,2 à 45°**	Projet :	**VIRGO Ncal**
CNRS - IN2P3 ULP IPHC Institut Pluridisciplinaire Hubert CURIEN STRASBOURG 23, rue du Loess - BP 28 67037 Strasbourg Cedex 02		ROTOR_S			
		Dessiné par : V. Zeter 19/11/2021	Vérifié par :	A3	Numéro	Echelle 1:2